Smart Mater. Struct. **19** (2010) 065025 (8pp) doi:10.1088/0964-1726/19/6/065025

An analytical solution for a multilayered magneto-electro-elastic circular plate under simply supported lateral boundary conditions

R Wang[1], Q Han[1,2] and E Pan[1]

[1] Computer Modelling and Simulation Group, College of Engineering, University of Akron, Akron, OH 44325-3905, USA
[2] School of Mechanical Engineering and Automation, Northeastern University, Shenyang 110004, People's Republic of China

E-mail: pan2@uakron.edu

Received 22 January 2010, in final form 16 April 2010
Published 11 May 2010
Online at stacks.iop.org/SMS/19/065025

Abstract
We derive, in this paper, the analytical solution for a three-dimensional transversely isotropic axisymmetric multilayered magneto-electro-elastic (MEE) circular plate under simply supported boundary conditions. The state space vector, the finite Hankel transform and propagating matrix methods are utilized together to obtain the full-field solutions for the MEE plate made of piezoelectric (PE) and piezomagnetic (PM) layers. Numerical examples for three-layered and five-layered PE/PM composites with different stacking sequences and under different loading conditions are presented and discussed. These results can serve as benchmark solutions for future numerical analyses of layered MEE plates.

(Some figures in this article are in colour only in the electronic version)

1. Introduction

Magneto-electro-elastic (MEE) coupling effect exists in multiphase materials which possess the ability to convert energy from one form to another (among elastic, electric and magnetic forms). Intensive studies on the physical and mechanical properties of the MEE structures were carried out by means of analytical, numerical and experimental methods. Among those MEE structures, the composites made of piezoelectric (PE) and piezomagnetic (PM) layers were frequently considered and some full-field exact solutions of these structures under certain boundary conditions were obtained. Pan and colleagues (Pan 2001, Pan and Heyliger 2002) derived the static and free vibration solutions for multilayered MEE rectangular plates under simply supported boundary conditions by using the Stroh formalism and propagating matrix method. By applying the state vector approach and propagating matrix method, Wang *et al* (2003) derived the exact solution of the multilayered MEE plate under static deformation, Chen *et al* (2005) extended the static solution to the vibration case, and Chen *et al* (2007) carried out the modal analysis of multilayered MEE plates. Combining the discrete layer approach and Ritz method, Ramirez *et al* (2006) derived an approximate solution for the free vibration of two-dimensional MEE laminate under both simply supported and fixed boundary conditions. Pan and Heyliger (2003) also derived exact solutions for MEE laminates under cylindrical bending. It can be seen that these solutions for the MEE coupling structures are all derived for the rectangular plates using the Cartesian coordinates.

The problem of a simply supported circular and homogeneous MEE plate under a uniform load was solved by Chen *et al* (2003) using four harmonic displacement functions. Chen *et al* (2006) also solved the free vibration problem of multilayered MEE composites where the dependence of natural frequencies on the thickness ratio was investigated. However there is no existing literature on the full-field solutions, especially on the field distribution along the thickness direction of multilayered MEE circular composites. For the reduced cases (elastic, piezoelectric or thin plate),

Deresiewicz and Mindlin (1955) and Deresiewicz (1956) obtained the analytical solution for axisymmetric elastic circular plates with free and clamped boundary conditions. Wang *et al* (2001) discussed the vibration problem of a piezoelectric circular laminate under simply supported and clamped boundary conditions based on the Kirchhoff thin plate theory. Ding *et al* (1999a, 1999b, 1999c) derived the exact solution for a piezoelectric circular plate under static and vibration conditions employing the state vector approach, finite Hankel transformation and propagating matrix method.

In this paper, Ding's approach is extended from the piezoelectric coupled plate to the MEE coupling one. Starting from the equilibrium equations for each homogeneous layer and making use of the geometric and constitutive equations, we first obtain a system of differential equations with separated derivatives with respect to the horizontal and vertical coordinates. Then, by employing the finite Hankel transform to suppress the horizontal coordinates, we arrive at a system of first-order differential equations which are easily solved. The solution for the layered MEE plate is expressed in terms of the propagating matrix and the inverse Hankel transformation is then applied to transform the solution from the Hankel domain back to the physical domain. Numerical examples are carried to show the effect of multiphase coupling and stacking sequence on the field distributions, which can be also served as benchmarks.

2. Basic equations

For a transversely isotropic MEE coupling solid with its material axis parallel to z-axis, the general constitutive equation can be expressed as:

$$\begin{Bmatrix} \sigma \\ D \\ B \end{Bmatrix} = \begin{bmatrix} C & -e & -q \\ e^{\mathrm{T}} & \varepsilon & \alpha \\ q^{\mathrm{T}} & \alpha^{\mathrm{T}} & \mu \end{bmatrix} \begin{Bmatrix} \gamma \\ E \\ H \end{Bmatrix} \tag{1}$$

where σ, D and B are the vectors of the elastic stress, electric displacement and magnetic induction; γ, E and H are the vectors of the elastic strain, electric field and magnetic field. These vectors are defined as

$$\sigma = \begin{Bmatrix} \sigma_r \\ \sigma_\theta \\ \sigma_z \\ \sigma_{rz} \end{Bmatrix}, \qquad D = \begin{Bmatrix} D_r \\ D_z \end{Bmatrix}, \qquad B = \begin{Bmatrix} B_r \\ B_z \end{Bmatrix},$$
$$\gamma = \begin{Bmatrix} \gamma_r \\ \gamma_\theta \\ \gamma_z \\ \gamma_{rz} \end{Bmatrix}, \qquad E = \begin{Bmatrix} E_r \\ E_z \end{Bmatrix}, \qquad H = \begin{Bmatrix} H_r \\ H_z \end{Bmatrix}. \tag{2}$$

Also in equation (1), C, e, q, ε, μ and α are, respectively, the matrices of the elastic stiffness, PE coefficients, PM coefficients, permittivity coefficients, permeability coefficients and magneto-electric (ME) coefficients. The elements of these matrices are

$$C = \begin{bmatrix} c_{11} & c_{12} & c_{13} & 0 \\ & c_{11} & c_{13} & 0 \\ & & c_{33} & 0 \\ & \text{sym} & & c_{44} \end{bmatrix}, \qquad e = \begin{bmatrix} 0 & e_{13} \\ 0 & e_{23} \\ 0 & e_{33} \\ e_{51} & 0 \end{bmatrix},$$
$$q = \begin{bmatrix} 0 & q_{13} \\ 0 & q_{23} \\ 0 & q_{33} \\ q_{51} & 0 \end{bmatrix} \tag{3a}$$
$$\varepsilon = \begin{bmatrix} \varepsilon_{11} & 0 \\ 0 & \varepsilon_{33} \end{bmatrix}, \qquad \mu = \begin{bmatrix} \mu_{11} & 0 \\ 0 & \mu_{22} \end{bmatrix},$$
$$\alpha = \begin{bmatrix} \alpha_{11} & 0 \\ 0 & \alpha_{33} \end{bmatrix}. \tag{3b}$$

Note that for the PE/PM layered structure α matrix is always zero; and for the PE layer q matrix is zero and for the PM layer e matrix is zero.

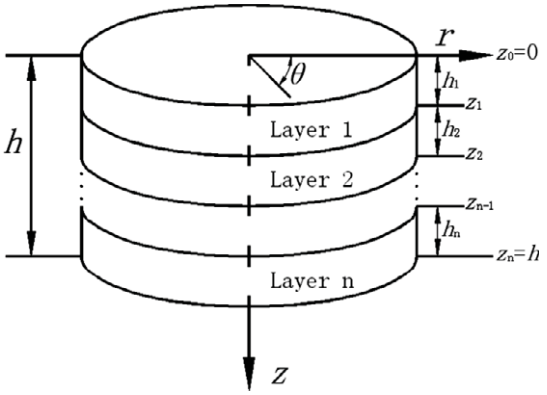

Figure 1. An n-layered circular plate with each layer being either PE or PM material.

The three-dimensional multilayered MEE circular plate model is shown in figure 1 in terms of the polar coordinates (r, θ, z). Since the problem is axisymmetric, the solution is θ-independent. The general geometric equation for the non-zero quantities can be expressed as

$$\gamma_r = \frac{\partial u}{\partial r} \qquad \gamma_\theta = \frac{u}{r} \qquad \gamma_z = \frac{\partial w}{\partial z} \qquad \gamma_{rz} = \frac{\partial u}{\partial z} + \frac{\partial w}{\partial r},$$
$$E_r = -\frac{\partial \phi}{\partial r} \qquad E_z = -\frac{\partial \phi}{\partial z}$$
$$H_r = -\frac{\partial \psi}{\partial r} \qquad H_z = -\frac{\partial \psi}{\partial z} \tag{4}$$

where u, w, ϕ and ψ are, respectively, the displacement in r- and z-directions, and the electric and magnetic potentials.

The equilibrium equations without body force, electric and magnetic charges can be expressed as

$$\frac{\partial \sigma_r}{\partial r} + \frac{\sigma_{rz}}{\partial z} + \frac{\sigma_r - \sigma_\theta}{r} = 0 \qquad \frac{\partial \sigma_{rz}}{\partial r} + \frac{\partial \sigma_z}{\partial z} + \frac{\sigma_{rz}}{r} = 0$$
$$\frac{\partial D_r}{\partial r} + \frac{\partial D_z}{\partial z} + \frac{D_r}{r} = 0 \qquad \frac{\partial B_r}{\partial r} + \frac{\partial B_z}{\partial z} + \frac{B_r}{r} = 0. \tag{5}$$

3. General solutions

Following Ding *et al* (1999a, 1999c), we define the following dimensionless variables:

$$\xi = r/a, \qquad \zeta = z/h, \qquad \bar{u} = u/h,$$
$$\bar{w} = w/h, \qquad \bar{\phi} = \phi\sqrt{\varepsilon_{33}^{(1)}/c_{11}^{(1)}}/h,$$
$$\bar{\psi} = \psi\sqrt{\mu_{33}^{(1)}/c_{11}^{(1)}}/h \qquad \bar{\sigma}_r = \sigma_r/c_{11}^{(1)}, \qquad \bar{\sigma}_z = \sigma_z/c_{11}^{(1)},$$
$$\bar{\sigma}_\theta = \sigma_\theta/c_{11}^{(1)}, \qquad \bar{\sigma}_{rz} = \sigma_{rz}/c_{11}^{(1)},$$
$$\bar{D}_r = D_r \Big/ \sqrt{\varepsilon_{33}^{(1)} c_{11}^{(1)}} \qquad \bar{D}_z = D_z \Big/ \sqrt{\varepsilon_{33}^{(1)} c_{11}^{(1)}},$$
$$\bar{B}_r = B_r \Big/ \sqrt{\mu_{33}^{(1)} c_{11}^{(1)}}, \qquad \bar{B}_z = B_z \Big/ \sqrt{\mu_{33}^{(1)} c_{11}^{(1)}} \tag{6}$$

where h and a are, respectively, the total thickness and radius of the plate; $c_{11}^{(1)}$, $\varepsilon_{11}^{(1)}$ and $\mu_{11}^{(1)}$ are, respectively, the elastic stiffness, electric permittivity and magnetic permeability constants of the first layer material.

By choosing the primary variables as the state space vector and rearranging equations (1), (4) and (5), we arrive at the following state equation

$$\frac{\partial \bar{\boldsymbol{R}}(\xi,\zeta)}{\partial \zeta} = \boldsymbol{A}\bar{\boldsymbol{R}}(\xi,\zeta) \tag{7}$$

where

$$\bar{\boldsymbol{R}}(\xi,\zeta) \equiv [\,\bar{u}(\xi,\zeta) \quad \bar{\sigma}_z(\xi,\zeta) \quad \bar{D}_z(\xi,\zeta) \quad \bar{B}_z(\xi,\zeta) \quad \bar{\sigma}_{rz}(\xi,\zeta) \quad \bar{w}(\xi,\zeta) \quad \bar{\phi}(\xi,\zeta) \quad \bar{\psi}(\xi,\zeta)\,]^{\mathrm{T}} \tag{8}$$

and $\boldsymbol{A}$ is a 8×8 operator matrix shown below.

$$\boldsymbol{A} = \begin{bmatrix} 0 & 0 & 0 & 0 \\ 0 & 0 & 0 & 0 \\ 0 & 0 & 0 & 0 \\ 0 & 0 & 0 & 0 \\ g_1\left(\frac{\partial^2}{\partial\xi^2} + \frac{1}{\xi}\frac{\partial}{\partial\xi} - \frac{1}{\xi^2}\right) & g_2\frac{\partial}{\partial\xi} & g_3\frac{\partial}{\partial\xi} & g_4\frac{\partial}{\partial\xi} \\ g_2\left(\frac{\partial}{\partial\xi} + \frac{1}{\xi}\right) & g_5 & g_6 & g_7 \\ g_3\left(\frac{\partial}{\partial\xi} + \frac{1}{\xi}\right) & g_8 & g_9 & g_{10} \\ g_4\left(\frac{\partial}{\partial\xi} + \frac{1}{\xi}\right) & g_7 & g_{10} & g_{11} \end{bmatrix}$$

$$\begin{bmatrix} f_1 & -s\frac{\partial}{\partial\xi} & f_2\frac{\partial}{\partial\xi} & f_3\frac{\partial}{\partial\xi} \\ -s\left(\frac{1}{\xi} + \frac{\partial}{\partial\xi}\right) & 0 & 0 & 0 \\ f_2\left(\frac{1}{\xi} + \frac{\partial}{\partial\xi}\right) & 0 & f_4\left(\frac{1}{\xi}\frac{\partial}{\partial\xi} + \frac{\partial^2}{\partial\xi^2}\right) & f_5\left(\frac{1}{\xi}\frac{\partial}{\partial\xi} + \frac{\partial^2}{\partial\xi^2}\right) \\ f_3\left(\frac{1}{\xi} + \frac{\partial}{\partial\xi}\right) & 0 & f_5\left(\frac{1}{\xi}\frac{\partial}{\partial\xi} + \frac{\partial^2}{\partial\xi^2}\right) & f_6\left(\frac{1}{\xi}\frac{\partial}{\partial\xi} + \frac{\partial^2}{\partial\xi^2}\right) \\ 0 & 0 & 0 & 0 \\ 0 & 0 & 0 & 0 \\ 0 & 0 & 0 & 0 \\ 0 & 0 & 0 & 0 \end{bmatrix}. \tag{9}$$

The secondary (or deduced) variables are expressed as

$$\begin{aligned}
&\bar{D}_r(\xi,\zeta) \\
&\quad = -\frac{1}{s}\left(f_2\bar{\sigma}_{rz}(\xi,\zeta) + f_4\frac{\partial\bar{\phi}(\xi,\zeta)}{\partial\xi} + f_5\frac{\partial\bar{\psi}(\xi,\zeta)}{\partial\xi}\right) \\
&\bar{B}_r(\xi,\zeta) \\
&\quad = -\frac{1}{s}\left(f_3\bar{\sigma}_{rz}(\xi,\zeta) + f_5\frac{\partial\bar{\phi}(\xi,\zeta)}{\partial\xi} + f_6\frac{\partial\bar{\psi}(\xi,\zeta)}{\partial\xi}\right) \\
&\bar{\sigma}_r(\xi,\zeta) \\
&\quad = -\frac{1}{s}\left(g_2\bar{\sigma}_z + g_3\bar{D}_z + g_4\bar{B}_z + g_1\frac{\partial\bar{u}_r(\xi,\zeta)}{\partial\xi} + l_1\frac{\bar{u}_r(\xi,\zeta)}{\xi}\right) \\
&\bar{\sigma}_\theta(\xi,\zeta) \\
&\quad = -\frac{1}{s}\left(g_2\bar{\sigma}_z + g_3\bar{D}_z + g_4\bar{B}_z + l_1\frac{\partial\bar{u}_r(\xi,\zeta)}{\partial\xi} + g_1\frac{\bar{u}_r(\xi,\zeta)}{\xi}\right)
\end{aligned} \tag{10}$$

where $\xi \in [0, 1]$, $\zeta \in [0, h_j/h]$ and h_j is the thickness of jth layer. Note that ζ is the local coordinate for each layer. The parameters in equations (9) and (10) are listed in the appendix.

Define the following finite Hankel transform of $f(\xi, \zeta)$ with respect to variable ξ as

$$f(k,\zeta) = \int_0^1 \xi f(\xi,\zeta) J_\mu(k\xi)\,\mathrm{d}\xi \tag{11}$$

where $J_\mu(k\xi)$ is the first kind of Bessel function of μth order. Then, the space vector in Hankel transform domain can be written as

$$\boldsymbol{R}(k,\zeta) = \begin{Bmatrix} U(k,\zeta) \\ S(k,\zeta) \\ D(k,\zeta) \\ B(k,\zeta) \\ T(k,\zeta) \\ W(k,\zeta) \\ F(k,\zeta) \\ P(k,\zeta) \end{Bmatrix} \equiv \begin{Bmatrix} J_1(\bar{u}_r(\xi,\zeta)) \\ J_0(\bar{\sigma}_z(\xi,\zeta)) \\ J_0(\bar{D}_z(\xi,\zeta)) \\ J_0(\bar{B}_z(\xi,\zeta)) \\ J_1(\bar{\sigma}_{rz}(\xi,\zeta)) \\ J_0(\bar{u}_z(\xi,\zeta)) \\ J_0(\bar{\phi}(\xi,\zeta)) \\ J_0(\bar{\psi}(\xi,\zeta)) \end{Bmatrix}. \tag{12}$$

Applying the Hankel transform to both sides of equation (7), we obtain

$$\frac{\partial \boldsymbol{R}(k,\zeta)}{\partial\zeta} = \boldsymbol{K}(k)\boldsymbol{R}(k,\zeta) + \boldsymbol{Q}(k,\zeta) \tag{13}$$

where

$$\boldsymbol{K}(k) = \begin{bmatrix} 0 & 0 & 0 & 0 & f_1 & sk & -f_2k & -f_3k \\ 0 & 0 & 0 & 0 & -sk & 0 & 0 & 0 \\ 0 & 0 & 0 & 0 & f_2k & 0 & -f_4k^2 & -f_5k^2 \\ 0 & 0 & 0 & 0 & f_3k & 0 & -f_5k^2 & -f_6k^2 \\ -g_1k^2 & -g_2k & -g_3k & -g_4k & 0 & 0 & 0 & 0 \\ g_2k & g_5 & g_6 & g_7 & 0 & 0 & 0 & 0 \\ g_3k & g_8 & g_9 & g_{10} & 0 & 0 & 0 & 0 \\ g_4k & g_7 & g_{10} & g_{11} & 0 & 0 & 0 & 0 \end{bmatrix} \tag{14}$$

and

$$\boldsymbol{Q}(k) = \left\{ \begin{array}{c} -s\bar{w}(1,\zeta)J_1(k) + f_2\bar{\phi}(1,\zeta)J_1(k) + f_3\bar{\psi}(1,\zeta)J_1(k) \\ -s\bar{\sigma}_{rz}(1,\zeta)J_0(k) \\ (kf_4\bar{\phi}(1,\zeta) + kf_6\bar{\psi}(1,\zeta))J_1(k) + (f_2\bar{\sigma}_{rz}(1,\zeta) - f_4\bar{E}_r(1,\zeta) - f_5\bar{H}_r(1,\zeta))J_0(k) \\ (kf_5\bar{\phi}(1,\zeta) + kf_6\bar{\psi}(1,\zeta))J_1(k) + (f_3\bar{\sigma}_{rz}(1,\zeta) - f_5\bar{E}_r(1,\zeta) - f_6\bar{H}_r(1,\zeta))J_0(k) \\ (g_1\bar{u}(1,\zeta) + g_1\bar{\varepsilon}_r(1,\zeta) + g_2\bar{\sigma}_z(1,\zeta) + g_3\bar{D}_z(1,\zeta) + g_4\bar{B}_z(1,\zeta))J_1(k) - kg_1\bar{u}(1,\zeta)J_0(k) \\ g_2\bar{u}(1,\zeta)J_0(k) \\ g_3\bar{u}(1,\zeta)J_0(k) \\ g_4\bar{u}(1,\zeta)J_0(k) \end{array} \right\} \tag{15}$$

with both $\boldsymbol{K}$ and $\boldsymbol{Q}$ depending also on the material properties.

From equation (10), we note that

$$\begin{aligned} s\bar{D}_r(1,\zeta) &= -f_2\bar{\sigma}_{rz}(\xi,\zeta) + f_4\bar{E}_r(1,\zeta) + f_5\bar{H}_r(1,\zeta) \\ s\bar{B}_r(\xi,\zeta) &= -f_3\bar{\sigma}_{rz}(\xi,\zeta) + f_5\bar{E}_r(1,\zeta) + f_6\bar{H}_r(1,\zeta) \\ s\bar{\sigma}_r(1,\zeta) &= -(g_2\bar{\sigma}_z + g_3\bar{D}_z + g_4\bar{B}_z + g_1\bar{\varepsilon}_r(1,\zeta) + l_1\bar{u}_r(1,\zeta)). \end{aligned} \tag{16}$$

Substituting equation (16) into (15) gives

$$\boldsymbol{Q}(k) = \left\{ \begin{array}{c} -s\bar{w}(1,\zeta)J_1(k) + f_2\bar{\phi}(1,\zeta)J_1(k) + f_3\bar{\psi}(1,\zeta)J_1(k) \\ -s\bar{\sigma}_{rz}(1,\zeta)J_0(k) \\ (kf_4\bar{\phi}(1,\zeta) + kf_6\bar{\psi}(1,\zeta))J_1(k) - s\bar{D}_r(1,\zeta)J_0(k) \\ (kf_5\bar{\varphi}(1,\zeta) + kf_6\bar{\psi}(1,\zeta))J_1(k) - s\bar{B}_r(1,\zeta)J_0(k) \\ (-s\bar{\sigma}_r(1,\zeta) + \frac{c_{11}-c_{12}}{c_{11}^{(1)}}s^2\bar{u}(1,\zeta))J_1(k) - kg_1\bar{u}(1,\zeta)J_0(k) \\ g_2\bar{u}(1,\zeta)J_0(k) \\ g_3\bar{u}(1,\zeta)J_0(k) \\ g_4\bar{u}(1,\zeta)J_0(k) \end{array} \right\}. \tag{17}$$

We now consider the simply supported lateral boundary condition at $\xi = 1$ (Ding *et al* 1999a, 1999c), i.e.,

$$\begin{aligned} &\bar{w}(1,\zeta) = 0, \qquad \bar{\phi}(1,\zeta) = 0, \qquad \bar{\psi}(1,\zeta) = 0, \\ &J_0(k) = 0 \qquad \frac{c_{11}-c_{12}}{c_{11}^{(1)}}s\bar{u}(1,\zeta) + \bar{\sigma}_r(1,\zeta) = 0. \end{aligned} \tag{18}$$

Then the column matrix $Q(k)$ vanishes and equation (13) becomes a homogeneous set of equations and its solution can be assumed in the following exponential form

$$\boldsymbol{R}(k,\zeta) = \boldsymbol{T}(k,\zeta)\boldsymbol{R}(k,0) \tag{19}$$

where

$$\boldsymbol{T}(k,\zeta) = \exp(\boldsymbol{K}(k)\zeta) \tag{20}$$

is called the propagator, or propagating matrix and varies along the vertical coordinate. It relates the values of space vector at arbitrary height ζ to that at the top surface of the layer.

Considering the continuity on the layer interface of two adjacent layers, say at $z = z_j$ between layers j and $j+1$, then the space vectors satisfy the following relation:

$$R_{j+1}(k,0) = R_j(k, z_j/h), \qquad j = 1, 2, \ldots, N. \tag{21}$$

Making use of the boundary conditions on the top and bottom surfaces of the layered plate, the space vectors can be related by

$$\boldsymbol{R}_n(k, h_n/h) = \boldsymbol{F}(k)\boldsymbol{R}_1(k,0) \tag{22}$$

where

$$\boldsymbol{F}(k) = \prod_{j=1}^{N} \boldsymbol{T}_j(k, h_j/h). \tag{23}$$

4. Loading conditions on the boundary

The general loading condition can be applied on the top and bottom surfaces in terms of the combination of prescribed elastic traction (σ_z and σ_{rz}) or elastic displacement (u and w), electric potential (ϕ) or electric displacement (D_z), and magnetic potential (ψ) or magnetic induction (B_z). There are totally eight prescribed quantities on both the top and bottom surfaces, and the remaining eight unknown quantities on these two surfaces can be determined. We assume that the dimensionless boundary conditions at the top and bottom surfaces are, respectively, as

$$\begin{aligned} \left\{ \begin{array}{c} \bar{\sigma}_z(\xi,0) \\ \bar{\sigma}_{rz}(\xi,0) \\ \bar{\phi}(\xi,0) \\ \bar{\psi}(\xi,0) \end{array} \right\}_{j=1} &= \left\{ \begin{array}{c} p_0(\xi) \\ q_0(\xi) \\ \phi_0(\xi) \\ \psi_0(\xi) \end{array} \right\} \\ \left\{ \begin{array}{c} \bar{\sigma}_z(\xi,1) \\ \bar{\sigma}_{rz}(\xi,1) \\ \bar{\phi}(\xi,1) \\ \bar{\psi}(\xi,1) \end{array} \right\}_{j=N} &= \left\{ \begin{array}{c} p_1(\xi) \\ q_1(\xi) \\ \phi_1(\xi) \\ \psi_1(\xi) \end{array} \right\}. \end{aligned} \tag{24}$$

By applying the Hankel transform (11) to the above prescribed loads, we obtain the loading conditions in Hankel domain

$$\begin{aligned} S(k,0) &= \int_0^1 \xi p_0(\xi) J_0(k\xi)\,\mathrm{d}\xi \\ T(k,0) &= \int_0^1 \xi q_0(\xi) J_0(k\xi)\,\mathrm{d}\xi \\ F(k,0) &= \int_0^1 \xi \phi_0(\xi) J_0(k\xi)\,\mathrm{d}\xi \\ P(k,0) &= \int_0^1 \xi \psi_0(\xi) J_0(k\xi)\,\mathrm{d}\xi \end{aligned} \tag{25a}$$

and

$$\begin{aligned} S(k,1) &= \int_0^1 \xi p_1(\xi) J_0(k\xi)\,\mathrm{d}\xi \\ T(k,1) &= \int_0^1 \xi q_1(\xi) J_0(k\xi)\,\mathrm{d}\xi \\ F(k,1) &= \int_0^1 \xi \phi_1(\xi) J_0(k\xi)\,\mathrm{d}\xi \\ P(k,1) &= \int_0^1 \xi \psi_1(\xi) J_0(k\xi)\,\mathrm{d}\xi. \end{aligned} \tag{25b}$$

From equation (22), the four unknowns on the top surface in Hankel domain can be determined as

$$\begin{Bmatrix} U(k,0) \\ D(k,0) \\ B(k,0) \\ W(k,0) \end{Bmatrix} = \begin{bmatrix} F_{21} & F_{23} & F_{24} & F_{26} \\ F_{51} & F_{53} & F_{54} & F_{56} \\ F_{71} & F_{73} & F_{74} & F_{76} \\ F_{81} & F_{83} & F_{84} & F_{86} \end{bmatrix}^{-1} \begin{Bmatrix} S(k,1) \\ T(k,1) \\ F(k,1) \\ P(k,1) \end{Bmatrix} - \begin{bmatrix} F_{21} & F_{23} & F_{24} & F_{26} \\ F_{51} & F_{53} & F_{54} & F_{56} \\ F_{71} & F_{73} & F_{74} & F_{76} \\ F_{81} & F_{83} & F_{84} & F_{86} \end{bmatrix}^{-1} \begin{bmatrix} F_{22} & F_{25} & F_{27} & F_{28} \\ F_{52} & F_{55} & F_{57} & F_{58} \\ F_{72} & F_{75} & F_{77} & F_{78} \\ F_{82} & F_{85} & F_{87} & F_{88} \end{bmatrix} \times \begin{Bmatrix} S(k,0) \\ T(k,0) \\ F(k,0) \\ P(k,0) \end{Bmatrix}. \tag{26}$$

Thus, $\boldsymbol{R}_1(k,0)$ is completely determined. Then equation (19) can be applied to determine $\boldsymbol{R}_j(k,\zeta)$ in any given layer j by the propagating relation, including those unknowns on the bottom surface.

Therefore, we have solved the layered MEE plate problem in the Hankel transformed domain. In order to find the solutions in the physical domain, we apply the inverse Hankel transform (Sneddon 1995):

$$\begin{aligned} \bar{u}(\xi,\zeta) &= 2\sum_i U(k_i,\zeta)\frac{J_1(k_i\xi)}{[J_1(k_i)]^2}, \\ \bar{\sigma}_z(\xi,\zeta) &= 2\sum_i S(k_i,\zeta)\frac{J_0(k_i\xi)}{[J_1(k_i)]^2}, \\ \bar{D}_z(\xi,\zeta) &= 2\sum_i D(k_i,\zeta)\frac{J_0(k_i\xi)}{[J_1(k_i)]^2}, \\ \bar{B}_z(\xi,\zeta) &= 2\sum_i B(k_i,\zeta)\frac{J_0(k_i\xi)}{[J_1(k_i)]^2}, \\ \bar{\sigma}_{rz}(\xi,\zeta) &= 2\sum_i T(k_i,\zeta)\frac{J_1(k_i\xi)}{[J_1(k_i)]^2}, \\ \bar{w}(\xi,\zeta) &= 2\sum_i W(k_i,\zeta)\frac{J_0(k_i\xi)}{[J_1(k_i)]^2}, \\ \bar{\phi}(\xi,\zeta) &= 2\sum_i F(k_i,\zeta)\frac{J_0(k_i\xi)}{[J_1(k_i)]^2}, \\ \bar{\psi}(\xi,\zeta) &= 2\sum_i P(k_i,\zeta)\frac{J_0(k_i\xi)}{[J_1(k_i)]^2}. \end{aligned} \tag{27}$$

The secondary variables in the physical domain are determined as

$$\begin{aligned} \bar{D}_r(\xi,\zeta) &= -\frac{f_2}{s}\bar{\sigma}_{rz}(\xi,\zeta) + \frac{2f_4}{s}\sum_i k_i F(k_i,\zeta)\frac{J_1(k_i\xi)}{[J_1(k_i)]^2} + \frac{2f_5}{s}\sum_i k_i P(k_i,\zeta)\frac{J_1(k_i\xi)}{[J_1(k_i)]^2} \\ \bar{B}_r(\xi,\zeta) &= -\frac{f_3}{s}\bar{\sigma}_{rz}(\xi,\zeta) + \frac{2f_5}{s}\sum_i k_i F(k_i,\zeta)\frac{J_1(k_i\xi)}{[J_1(k_i)]^2} + \frac{2f_6}{s}\sum_i k_i P(k_i,\zeta)\frac{J_1(k_i\xi)}{[J_1(k_i)]^2} \end{aligned}$$

Table 1. Material properties of $BaTiO_3$ and $CoFe_2O_4$ (Pan 2001) (C_{ij}: elastic constants in GPa; e_{ij}: piezoelectric coefficients in N V^{-1} m^{-1}; q_{ij}: piezomagnetic coefficients in N A^{-1} m^{-1}; ε_{ij}: permittivity coefficients in 10^{-9} C V^{-1} m^{-1}; and μ_{ij}: permeability coefficients in 10^{-6} Wb A^{-1} m^{-1}).

	$BaTiO_3$	$CoFe_2O_4$		$BaTiO_3$	$CoFe_2O_4$
C_{11}	166	286	q_{13}	0	580.3
C_{12}	77	173	q_{23}	0	580.3
C_{13}	78	170.5	q_{33}	0	699.7
C_{22}	166	286	q_{42}	0	550
C_{23}	78	170.5	q_{51}	0	550
C_{33}	162	269.5	ε_{11}	11.2	0.08
C_{44}	43	45.3	ε_{22}	11.2	0.08
C_{55}	43	45.3	ε_{33}	12.6	0.093
C_{66}	44.5	56.5	μ_{11}	5	590
e_{13}	−4.4	0	μ_{22}	5	590
e_{23}	−4.4	0	μ_{33}	10	157
e_{33}	18.6	0			
e_{42}	11.6	0			
e_{51}	11.6	0			

$$\begin{aligned} \bar{\sigma}_r(\xi,\zeta) &= -\frac{g_2}{s}\bar{\sigma}_z(\xi,\zeta) - \frac{g_3}{s}\bar{D}_z(\xi,\zeta) - \frac{g_4}{s}\bar{B}_z(\xi,\zeta) - \frac{2g_1}{s}\sum_i k_i U(k_i,\zeta)\frac{J_0(k_i\xi)}{[J_1(k_i)]^2} + \frac{(c_{11}-c_{12})s}{c_{11}^{(1)}}\frac{\bar{u}_r(\xi,\zeta)}{\xi} \\ \bar{\sigma}_\theta(\xi,\zeta) &= -\frac{g_2}{s}\bar{\sigma}_z(\xi,\zeta) - \frac{g_3}{s}\bar{D}_z(\xi,\zeta) - \frac{g_4}{s}\bar{B}_z(\xi,\zeta) - \frac{2l_1}{s}\sum_i k_i U(k_i,\zeta)\frac{J_0(k_i\xi)}{[J_1(k_i)]^2} - \frac{(c_{11}-c_{12})s}{c_{11}^{(1)}}\frac{\bar{u}_r(\xi,\zeta)}{\xi}. \end{aligned} \tag{28}$$

5. Numerical examples

5.1. Three-layered sandwich MEE composite

We first consider a sandwich structure composed of PE material $BaTiO_3$ and PM material $CoFe_2O_4$. Following the convention of Pan (2001) (i.e., $B = BaTiO_3$, and $F = CoFe_2O_4$), we use BFB for the $BaTiO_3/CoFe_2O_4/BaTiO_3$ sandwich plate and FBF for the $CoFe_2O_4/BaTiO_3/CoFe_2O_4$ sandwich plate. The material properties are listed in table 1. The total thickness and radius of the plate are, respectively, 12 mm and 30 mm, with each layer having the same thickness. The normal pressure $\sigma_z = -1$ N m^{-2} and $\sigma_z = 1$ N m^{-2} are, respectively, applied on the top ($z = 0$) and bottom ($z = h$) surfaces whilst $\sigma_{rz} = D_z = B_z = 0$ on both the top and bottom surfaces (LC1). Figures 2–5 show the distributions of the primary variables along the thickness direction (via vertical coordinate ζ) at fixed horizontal location $\xi = 0.3$. Since the boundary condition and the layered material structure are both symmetric, we present the field distribution only in the top half or the bottom half of the plate. It is observed that while different stacking sequences (BFB and FBF) have no obvious effect on the stress distribution (figure 3), their effect on the other field quantities, particularly on the electric and magnetic fields is significant (figures 4 and 5).

5.2. Five-layered MEE composite

In the second example, we extend the sandwich structure to five-layered plates with two different symmetric stacking

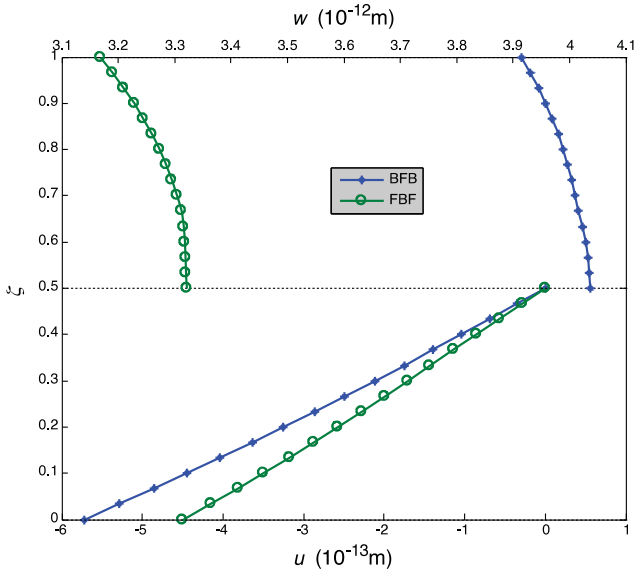

Figure 2. Variations of displacements along the thickness direction in three-layered BFB and FBF composites caused by the uniform mechanical pressures on the top and bottom surfaces under load condition LC1. Symmetric vertical displacement w in the top half and anti-symmetric radial displacement u in the bottom half of the plate.

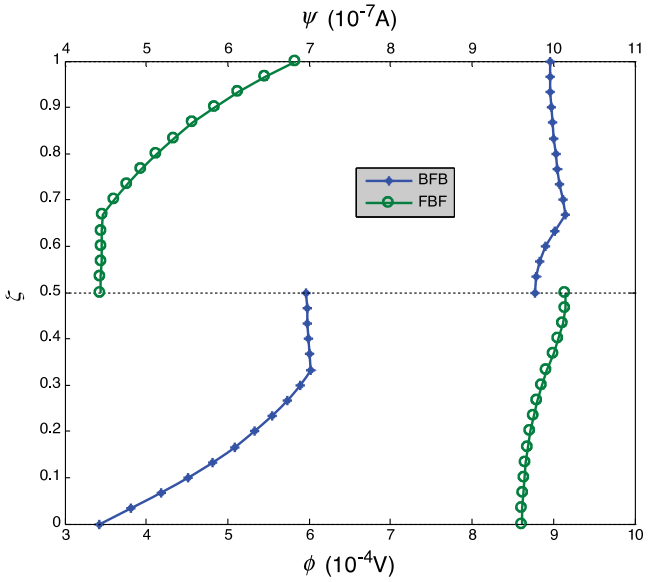

Figure 4. Variations of electric and magnetic potentials along the thickness direction in three-layered BFB and FBF composites caused by the uniform mechanical pressures on the top and bottom surfaces under load condition LC1. Symmetric electric potential ϕ in the bottom half and symmetric magnetic potential ψ in the top half of the plate.

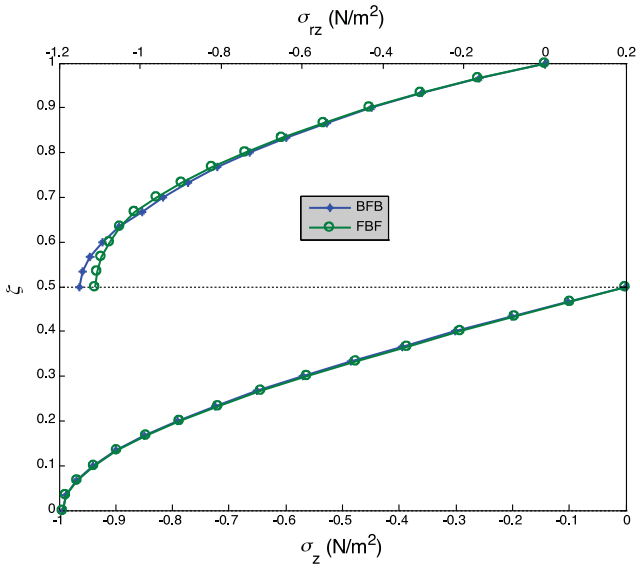

Figure 3. Variations of stress components along the thickness direction in three-layered BFB and FBF composites caused by the uniform mechanical pressures on the top and bottom surfaces under load condition LC1. Symmetric shear stress σ_{rz} in the top half and anti-symmetric normal stress σ_z in the bottom half of the plate.

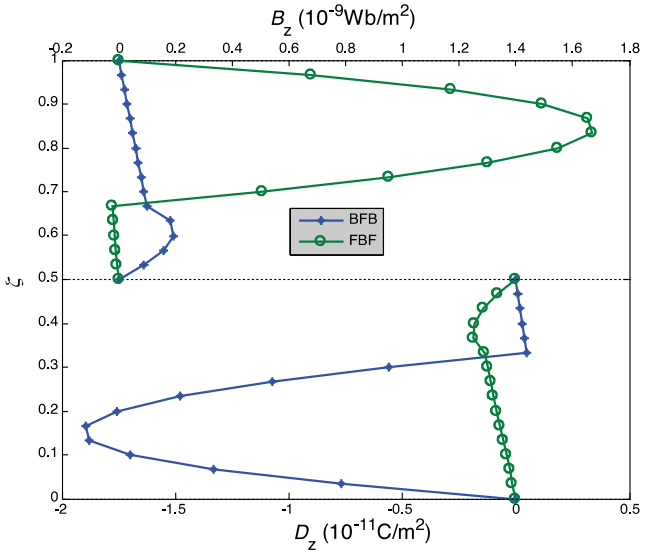

Figure 5. Variations of electric displacement and magnetic induction along the thickness direction in three-layered BFB and FBF composites caused by the uniform mechanical pressures on the top and bottom surfaces under load condition LC1. Anti-symmetric D_z in the bottom half and anti-symmetric B_z in the top half of the plate.

sequences: FBFBF and BFBFB. In this case, the total thickness is assumed to be 10 mm with each layer at 2 mm and the radius of the plate is still 30 mm. Similarly, the normal pressure is applied, with $\sigma_z = -1$ N m^{-2} at the top surface ($z = 0$) and $\sigma_z = 1$ N m^{-2} at the bottom surface ($z = h$). However, different to the first example, other boundary conditions at the top and bottom surfaces are $\sigma_{rz} = \phi = \psi = 0$ (LC2). Figures 6–9 show the distributions of the primary variables along the thickness direction (via vertical coordinate ζ) at fixed horizontal location $\xi = 0.3$. Compared to figures 2–5, we observe that the added layups and the altered boundary conditions influence only slightly the elastic field variations along the thickness direction (figures 2 and 3 versus figures 6 and 7). However, the layering and electric boundary condition can substantially affect the electric and magnetic field distributions (figures 4 and 5 versus figures 8 and 9).

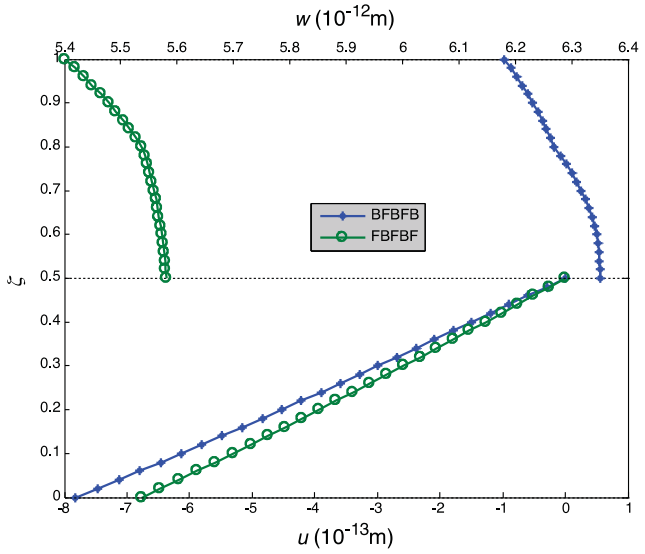

Figure 6. Variations of displacements along the thickness direction in five-layered BFBFB and FBFBF composites caused by the uniform mechanical pressures on the top and bottom surfaces under load condition LC2. Symmetric vertical displacement w in the top half and anti-symmetric radial displacement u in the bottom half of the plate.

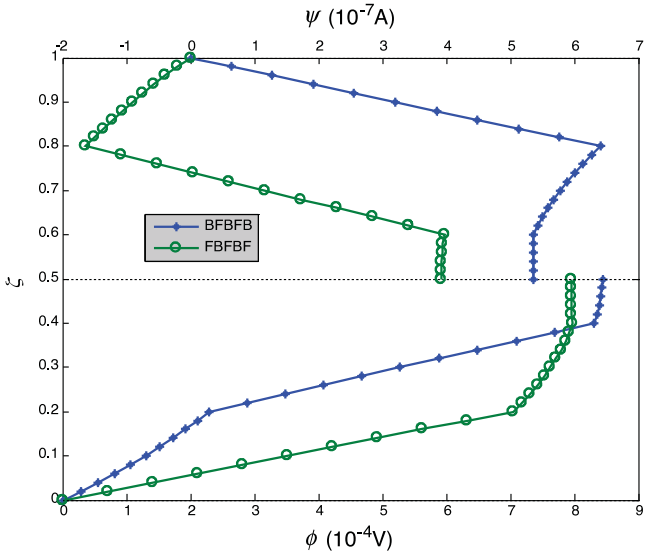

Figure 8. Variations of electric and magnetic potentials along the thickness direction in five-layered BFBFB and FBFBF composites caused by the uniform mechanical pressures on the top and bottom surfaces under load condition LC2. Symmetric electric potential ϕ in the bottom half and symmetric magnetic potential ψ in the top half of the plate.

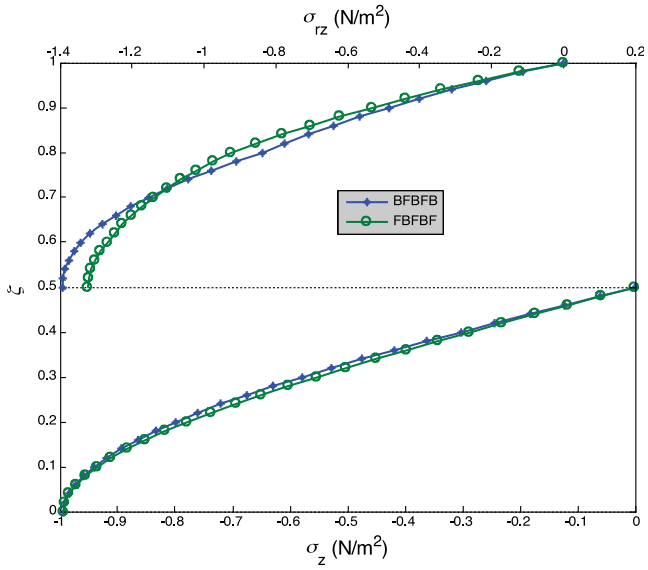

Figure 7. Variations of stress components along the thickness direction in five-layered BFBFB and FBFBF composites caused by the uniform mechanical pressures on the top and bottom surfaces under load condition LC2. Symmetric shear stress σ_{rz} in the top half and anti-symmetric normal stress σ_z in the bottom half of the plate.

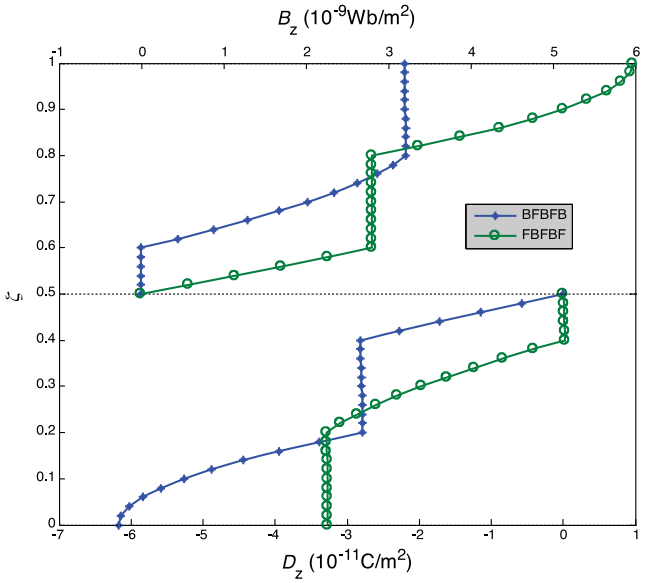

Figure 9. Variations of electric displacement and magnetic induction along the thickness direction in five-layered BFBFB and FBFBF composites caused by the uniform mechanical pressures on the top and bottom surfaces under load condition LC2. Anti-symmetric D_z in the bottom half and anti-symmetric B_z in the top half of the plate.

6. Conclusions

We derived an analytical solution for three-dimensional transversely isotropic axisymmetric multilayered magneto-electro-elastic (MEE) circular plates under simply supported lateral boundary conditions. The state space vector, finite Hankel transform and propagating matrix method are utilized to find the full-field solution for the MEE plate made of piezoelectric (PE) and piezomagnetic (PM) layers. Numerical examples for three-layered and five-layered PE/PM composites with different stacking sequences and under different boundary conditions are presented and discussed. Two different boundary conditions are applied on the top and bottom surfaces which show that the MEE layered composites with the electric/magnetic boundary conditions (i.e., the so-called electrodes/magnetrodes) can dramatically affect the field distribution of the electric (or magnetic) quantities. These results could be useful for the design of multilayered MEE composites and can be further served as benchmarks for future numerical analyses of layered MEE plates.

Acknowledgments

This work was partially supported by the Air Force Office of Scientific Research under grants AFOSR FA9550-06-1-0317 (EP, RW), and NSFC 50775028 (QH).

Appendix

$$s = h/a \qquad f_1 = c_{11}^{(1)}/c_{44} \qquad f_2 = -\frac{se_{15}}{c_{44}\sqrt{\varepsilon_{33}^{(1)}/c_{11}^{(1)}}}$$

$$f_3 = -\frac{sq_{15}}{c_{44}\sqrt{\mu_{33}^{(1)}/c_{11}^{(1)}}} \qquad f_4 = s^2(e_{15}^2/c_{44} + \varepsilon_{11})/\varepsilon_{33}^{(1)}$$

$$f_5 = s^2(e_{15}q_{15}/c_{44} + \alpha_{11})/\sqrt{\mu_{33}^{(1)}\varepsilon_{33}^{(1)}}$$

$$f_6 = s^2(q_{15}q_{15}/c_{44} + \mu_{11})/\mu_{33}^{(1)}$$

$$g_0 = c_{33}\varepsilon_{33}\mu_{33} + e_{33}e_{33}\mu_{33} + q_{33}\varepsilon_{33}q_{33}$$

$$g_1 = \frac{s^2}{c_{11}^{(a)}g_0}(e_{33}^2(q_{13}^2 + c_{11}\mu_{33}) - e_{13}e_{33}(q_{13}q_{33} + c_{13}\mu_{33}) + e_{13}^2(q_{33}^2 + c_{33}\mu_{33}) + \varepsilon_{33}(c_{33}q_{13}^2 - 2c_{13}q_{13}q_{33} + c_{11}q_{33}^2 - c_{13}^2\mu_{33} + c_{11}c_{33}\mu_{33}))$$

$$g_2 = s(-c_{13}\varepsilon_{33}\mu_{33} - e_{31}e_{33}\mu_{33} - q_{31}q_{33}\varepsilon_{33})/g_0$$

$$g_3 = s(c_{33}e_{31}\mu_{33} - c_{13}e_{33}\mu_{33} - e_{33}q_{31}q_{33} + e_{31}q_{33}^2) \times \sqrt{\varepsilon_{33}^{(1)}/c_{11}^{(1)}}/g_0$$

$$g_4 = -s(-e_{33}^2q_{31} - c_{33}\varepsilon_{33}q_{31} + e_{31}e_{33}q_{33} + c_{13}\varepsilon_{33}q_{33}) \times \sqrt{\mu_{33}^{(1)}/c_{11}^{(1)}}/g_0$$

$$g_5 = c_{11}^{(1)}\varepsilon_{33}\mu_{33}/g_0 \qquad g_6 = e_{33}\mu_{33}\sqrt{c_{11}^{(1)}\varepsilon_{33}^{(1)}}/g_0$$

$$g_7 = \varepsilon_{33}q_{33}\sqrt{c_{11}^{(1)}\mu_{33}^{(1)}}/g_0 \qquad g_8 = e_{33}\mu_{33}\sqrt{c_{11}^{(1)}\varepsilon_{33}^{(1)}}/g_0$$

$$g_9 = -(c_{33}\mu_{33} + q_{33}^2)\varepsilon_{33}^{(1)}/g_0 \qquad g_{10} = e_{33}q_{33}\sqrt{\mu_{33}^{(1)}\varepsilon_{33}^{(1)}}/g_0$$

$$g_{11} = -(e_{33}^2 + c_{33}\varepsilon_{33})\mu_{33}^{(1)}/g_0$$

$$l_1 = \frac{s^2}{c_{11}^{(a)}g_0}(e_{33}^2(q_{13}^2 + c_{12}\mu_{33}) - e_{13}e_{33}(q_{13}q_{33} + c_{13}\mu_{33}) + e_{13}^2(q_{33}^2 + c_{33}\mu_{33}) + \varepsilon_{33}(c_{33}q_{13}^2 - 2c_{13}q_{13}q_{33} + c_{12}q_{33}^2 - c_{13}^2\mu_{33} + c_{12}c_{33}\mu_{33})).$$

References

Chen J, Chen H, Pan E and Heyliger P R 2007 Modal analysis of magneto-electro-elastic plates using the state-vector approach *J. Sound Vib.* **304** 722–34

Chen J, Ding H and Hou P 2003 Analytical solutions of simply supported magnetoelectroelastic circular plate under uniform loads *J. Zhejiang Univ. Sci.* **4** 560–4

Chen J, Xu R, Huang X and Ding H 2006 Exact solutions of axisymmetric free vibration of transversely isotropic magnetoelectroelastic laminated circular plates *Struct. Eng. Mech.* **23** 115–27

Chen W Q, Lee K Y and Ding H J 2005 On free vibration of non-homogeneous transversely isotropic magneto-electro-elastic plates *J. Sound Vib.* **279** 237–51

Deresiewicz H 1956 Symmetric flexural vibrations of a clamped circular disc *J. Appl. Mech.* **23** 319

Deresiewicz H and Mindlin R D 1955 Axially symmetric flexural vibrations of a circular disc *J. Appl. Mech.* **22** 86–8

Ding H, Xu R and Lin F 1999a Exact solution for axisymmetric transversely isotropic piezoelectric circular plate—I. Exact solution for the piezoelectric circular plate (in Chinese) *Sci. China* E **29** 214–21

Ding H, Xu R and Lin F 1999b Exact solution for axisymmetric transversely isotropic piezoelectric circular plate—II. Exact solution and numerical example for the elastic circular plate (in Chinese) *Sci. China* E **29** 298–305

Ding H, Xu R, Chi Y and Chen W 1999c Free axisymmetric vibration of transversely isotropic piezoelectric circular plates *Int. J. Solids Struct.* **36** 4629–52

Pan E 2001 Exact solution for simply supported and multilayered magneto-electro-elastic plates *J. Appl. Mech. Trans. ASME* **68** 608–18

Pan E and Heyliger P R 2002 Free vibrations of simply supported and multilayered magneto-electro-elastic plates *J. Sound Vib.* **252** 429–42

Pan E and Heyliger P R 2003 Exact solutions for magneto-electro-elastic laminates in cylindrical bending *Int. J. Solids Struct.* **40** 6859–76

Ramirez F, Heyliger P R and Pan E 2006 Free vibration response of two-dimensional magneto-electro-elastic laminated plates *J. Sound Vib.* **292** 626–44

Sneddon I N 1995 *Fourier Transform* (New York: Dover) pp 82–91

Wang J, Chen L and Fang S 2003 State vector approach to analysis of multilayered magneto-electro-elastic plates *Int. J. Solids Struct.* **70** 1669–80

Wang Q, Quek S T, Sun C T and Liu X 2001 Analysis of piezoelectric coupled circular plate *Smart Mater. Struct.* **10** 229–39